

**MACS, AN INSTRUMENT, AND A METHODOLOGY FOR  
SIMULTANEOUS AND GLOBAL MEASUREMENTS OF THE CORONAL  
ELECTRON TEMPERATURE AND THE SOLAR WIND VELOCITY  
ON THE SOLAR CORONA**

**by**

**Nelson Leslie Reginald**

A dissertation submitted to the Faculty of the University of Delaware in partial fulfillment of the requirements for the degree of Doctor of Philosophy with a major in Physics

Fall 2000

© 2000 Nelson Leslie Reginald

All Rights Reserved

**MACS, AN INSTRUMENT, AND A METHODOLOGY FOR  
SIMULTANEOUS AND GLOBAL MEASUREMENTS OF THE CORONAL  
ELECTRON TEMPERATURE AND THE SOLAR WIND VELOCITY  
ON THE SOLAR CORONA**

by

**Nelson Leslie Reginald**

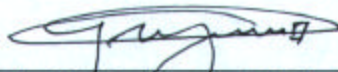
Approved: \_\_\_\_\_



Henry R. Glyde, Ph.D.

Chairman, Department of Physics and Astronomy

Approved: \_\_\_\_\_



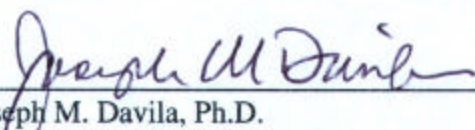
Conrado M. Gempesaw II, Ph.D.

Vice Provost for Academic Programs and Planning


I certify that I have read this dissertation and that in my opinion it meets the academic and professional standard required by the University as a dissertation for the degree of Doctor of Philosophy.

Signed:   
Dermott J. Mullan, Ph.D.  
Professor in charge of dissertation

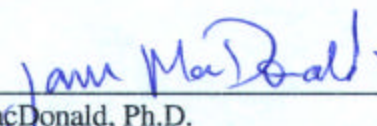
I certify that I have read this dissertation and that in my opinion it meets the academic and professional standard required by the University as a dissertation for the degree of Doctor of Philosophy.

Signed:   
Joseph M. Davila, Ph.D.  
Member of dissertation committee

I certify that I have read this dissertation and that in my opinion it meets the academic and professional standard required by the University as a dissertation for the degree of Doctor of Philosophy.

Signed:   
Stanley P. Owocki, Ph.D.  
Member of dissertation committee

I certify that I have read this dissertation and that in my opinion it meets the academic and professional standard required by the University as a dissertation for the degree of Doctor of Philosophy.

Signed:   
James MacDonald, Ph.D.  
Member of dissertation committee

I certify that I have read this dissertation and that in my opinion it meets the academic and professional standard required by the University as a dissertation for the degree of Doctor of Philosophy.

Signed:   
George H. Watson, Ph.D.  
Member of dissertation committee

## **Acknowledgements**

I am greatly proud for the opportunity afforded to conduct my Ph.D. dissertation research at the Solar Physics Division of the NASA's Goddard Space Flight Center in Greenbelt, Maryland, USA under the able guidance of Dr. Joseph M. Davila. I am also thankful for the opportunity provided to participate in the assembly of the SERTS (Solar Extreme Ultraviolet Rocket Telescope) payload and its launch on the 26 July 2000 from the White Sands Missile Range, New Mexico.

In this regard I wish to convey my hearty thanks to Dr. Dermott J. Mullan for the trust and faith in recommending me for the graduate research position offered by Dr. Davila, for providing the funds to attend the International Summer School on "The Sun As Seen From Space" in L'Aquila, Italy (1997) and for serving as the chairman of the Ph.D. thesis committee.

This research that spanned over the years 1998 to 2000 involved in the theoretical modeling, the design and construction of an instrument, an eclipse expedition to Turkey (1999), the analyses and travel to the AAS meetings in Chicago (1999) & Nevada (2000), the TRACE workshop in California (1999), the AGU conference in Washington D.C

(2000) and the IAP “Eclipses and the Solar Corona” conference in France (2000), thus molding me for a successful scientific career.

My sincere thanks are also extended to Mr. Chuck Condor for helping with all the encouragement and logistics for the eclipse expedition to Turkey, and to Mr. Larry White for the long hours spent on the engineering drawings and fabrication of MACS.

I also wish to convey my regards to the staff of my high school at S. Thomas’ College, Mount Lavinia, Sri Lanka and my undergraduate institute at the University of Peradeniya in Sri Lanka, my MS thesis advisor and chairman Prof. James MacDonald at the University of Delaware and for the full tuition scholarship and teaching assistantship awarded by the University of Delaware, which enabled me to travel to the USA in 1994 in pursuance with my graduate studies.

My sincere thanks is also extended to Miss. Elizabeth (Sugar Bug) Chapman for her help in preparing the text.

**Dedicated to my loving parents**  
**Gnaniah J. Reginald & Beryl A. Reginald**

## TABLE OF CONTENTS

LIST OF TABLES.....	xii
LIST OF FIGURES.....	xv
ABSTRACT.....	xxxviii
<b>Chapter</b>	
<b>1 INTRODUCTION.....</b>	<b>1</b>
1.1 Introduction to the solar corona.....	1
1.2 Other methods to measure the solar wind velocity and the coronal temperature.....	12
<b>2 FORMATION OF THE K-CORONA AND THE FOCUS OF THIS RESEARCH.....</b>	<b>18</b>
2.1 K-corona.....	18
2.2 The photospheric spectrum.....	18
2.3 The scattering source.....	20
2.4 The effects on the incident radiation by the scattering source.....	21
2.5 The K-coronal spectrum.....	22
2.6 Further explanation for the formation of the temperature sensitive anti- nodes.....	29

2.7	The influence of the solar wind on the K-coronal spectrum.....	38
2.8	Simultaneous determination of the coronal temperature and the solar wind velocity.....	44
2.9	Global determination of the coronal temperature and the solar wind velocity.....	47
2.10	The essence of this dissertation.....	48
<b>3</b>	<b>THE INSTRUMENT.....</b>	<b>49</b>
3.1	Overview of the instrument.....	49
3.2	Description of the optical elements in detail .....	58
3.2.1	The telescope.....	58
3.2.2	The fibers.....	61
3.2.3	The lenses.....	65
3.2.4	The grating.....	67
3.2.5	The camera.....	68
3.3	Analytical expressions for the integration time, the spectral resolution and the spatial resolution.....	69
3.4	Cost of the instrument .....	87
<b>4</b>	<b>OBSERVATIONAL RESULTS AND ANALYSES.....</b>	<b>88</b>
4.1	Observational site.....	88
4.2	Spectra observed by MACS.....	90
4.3	Identifying the individual fiber location on the corona.....	93



4.4	The telescope-spectrometer sensitivity curve .....	108
4.5	Application of the intensity correction factor .....	115
4.6	Determination of the Thermal electron temperature and the Solar wind velocity for each fiber location .....	116
4.7	Sources of error and error bars.....	132
4.8	Summary.....	135
<b>5</b>	<b>MODIFIED CRAM’S THEORY AND ITS DEPENDENCE ON VARIOUS PARAMETERS.....</b>	<b>136</b>
5.1	Modified Cram’s theory.....	136
5.2	Dependence on the electron density distribution function.....	140
5.3	Dependence on the temperature profile.....	155
5.4	Dependence on the wind profile.....	158
5.5	Dependence on the numerical method.....	162
<b>6</b>	<b>COMPARISON BETWEEN AND OBSERVATION AND THEORY.....</b>	<b>167</b>
6.1	An unexpected phenomenon noticed in the observations.....	167
6.2	Comparison between theory and observation.....	169
6.3	Remedial measures.....	179
<b>7</b>	<b>CONCLUSION.....</b>	<b>185</b>
7.1	Summary of this thesis.....	185
7.2	Using a space platform.....	188

## Appendix

<b>A</b>	<b>THE THEORY OF FORMATION OF THE K-CORONA.....</b>	<b>197</b>
A.1	The general theory of scattering of radiation by free electrons.....	197
A.2	The total power radiated per unit solid angle for the cases where the electric vector is aligned parallel and perpendicular to the scattering Plane.....	206
A.3	Contribution due to Compton scattering.....	216
A.4	Expression for the total K-coronal scattered intensity.....	218
A.5	Expressions for the dependent variables in equation (A.78) in terms of the independent variables.....	226
A.6	Expression for the incident solar intensity on the coronal electrons....	230
A.7	Final expression for the observed intensity.....	233
<b>B</b>	<b>CODE.....</b>	<b>235</b>
B.1	The basic equation to be solved.....	235
B.2	Approximations to the $\int d\lambda'$ integral.....	237
B.3	$b, Q_{//}^{Ra}$ and $Q_{\perp}^{Ra}$ in terms of the independent variables $\omega, \varphi$ and $x$ .....	239
B.4	Rewriting the basic equation with all parameters expressed in terms of the independent variables $(\omega, \varphi, x, y)$ .....	241
B.5	Changing the independent variable $\cos \omega$ to $\cos \theta$ .....	243
B.6	Expression for the extraterrestrial solar irradiance $f(\xi)$ .....	247
B.7	Expressions for the limb-darkening coefficient $u_1(\xi)$ .....	248

B.8	Expression for the coronal electron density model	
	$N_e \left( \sqrt{x^2 + \rho^2} R_{\text{solar}} \right)$ .....	<b>250</b>
B.9	Expressions for the coronal temperature model $T \left( \sqrt{x^2 + \rho^2} R_{\text{solar}} \right)$	
	and the solar wind model $W \left( \sqrt{x^2 + \rho^2} R_{\text{solar}} \right)$ .....	<b>251</b>
B.10	Evaluation of the integrals.....	<b>252</b>
B.11	The symbols used in the code.....	<b>264</b>
B.12	The IDL code.....	<b>267</b>
<b>C</b>	<b>A STREAMER MODEL</b> .....	<b>276</b>
C.1	The effects due to streamers.....	<b>276</b>
	<b>REFERENCES</b> .....	<b>285</b>

## LIST OF TABLES

3.1	A table showing the values for the angle of diffraction, the linear dispersion, the line width and the resolvable theoretical wavelength range for three different wavelengths using the physical parameters of the optical components used in MACS. In column 3 the reciprocal linear dispersion is calculated per pixel, which is the dimension of a pixel in the CCD camera used in MACS.....	<b>79</b>
3.2	The transmission efficiencies of the fibers, the lenses and the grating for three different wavelengths. This information is from figure (3.9), figure (3.11) and figure (3.12).....	<b>83</b>
3.3	The list of lenses and the associated number of surfaces through which the incident light had to pass before entering the detector.....	<b>83</b>
3.4	The effective transmission efficiency ( $t_1^{\text{eff}}$ ) of MACS for the wavelengths 3600.0, 4000.0 and 4500.0 angstroms. The values are based on the information from tables (3.2) and (3.3).....	<b>84</b>

3.5	The K-coronal brightness at 1.1 and 1.6 solar radii for three different wavelengths during the solar maximum. The values were obtained from Allen (1973) from pages 172 and 176. The units are in ergs/sec/cm <sup>2</sup> /angs/steradians. (1 Joule=10 <sup>7</sup> ergs).....	<b>84</b>
3.6	Lower limit of the integration time for the K-coronal spectrum for MACS based on equation (3.36).....	<b>85</b>
3.7	Cost associated with the construction of MACS.....	<b>87</b>
4.1	List of the emission lines reported by Athay and Orrall (1957) of a prominence from the total solar eclipse of 1952. In this paper the Sr II line at 4077.7 has been erroneously recorded as 3077.7 angstrom. In the following table only the emission lines that could lie within the wavelength range of MACS is enumerated.....	<b>96</b>
4.2	List of the emission lines reported by Jefferies, Smith and Smith (1959) from the flare of 18 September 1957. This table only includes those emission lines categorized as very strong and strong. Also in this following table only the emission lines that could lie within the wavelength range of MACS is enumerated.....	<b>100</b>
6.1	Comparison of the wind and the temperature sensitive intensity ratios between the observational and the theoretical K-coronal spectrum, for fiber #04. These values are based on figure (6.5).....	<b>177</b>

B.1	The dependence of the extraterrestrial solar irradiance and the limb-darkening functions with the wavelength. The columns 1 and 4 are from section (B.6) and columns 2 and 3 are from section (B.7).....	<b>259</b>
B.2	Cumulative values of the columns 2,3 and 4 of table (B.1).....	<b>260</b>
B.3	Multiplying column 4 of table (B.2) with column 2 and 3 of table (B.2). This is the format of the table used by the code.....	<b>260</b>
B.4	The format of the input information on the wind velocity in km/sec, isothermal temperature in MK and the distance to the line of sight in SR.....	<b>275</b>

## LIST OF FIGURES

1.1	The solar corona as seen during the solar eclipse of February 26, 1998. Picture: NASA eclipse library.....	<b>1</b>
1.2	This plot shows the variation of the E, K and F components of the solar coronal brightness with height above the solar limb.....	<b>7</b>
1.3	A cross section of the sun to highlight the prominent parts of it and the temperature scales between the core, photosphere and the corona. Picture: SOHO pictures library.....	<b>9</b>
2.1	This is a plot of the extraterrestrial solar irradiance spectrum. This was obtained by starting with the ground-based Fourier Transform Spectrometer at the McMath/Pierce Solar Telescope at Kitt Peak, Arizona, and then correcting for wavelength-dependent absorption in the Earth's atmosphere.....	<b>19</b>
2.2	The photospheric radiation is emitted from a point S on the surface of the sun. The electrons at point P in the corona scatter some of the incident radiation towards a terrestrial observer at E, which is known as K-coronal radiation.....	<b>23</b>

2.3	This plot shows the modeled K-coronal intensity spectra against wavelength. The composite plots are for different isothermal temperatures assumed for the solar corona for a given line of sight at 1.1 solar radii.....	24
2.4	Modeled K-coronal intensity spectrum against wavelength for different isothermal coronal temperatures for a given line of sight at 1.3 solar radii.....	25
2.5	Modeled K-coronal intensity spectrum against wavelength for different isothermal coronal temperatures for a given line of sight at 1.5 solar radii.....	26
2.6	This is a plot of the K-coronal intensity ratios at 3850 .0 to 4100.0 angstroms against the assumed isothermal coronal temperatures. The ratios were calculated from the modeled K-coronal spectra for different temperatures shown in figure (2.3). These values pertain to a line of sight at 1.1 solar radii.....	27
2.7	An input intensity spectrum containing an absorption line centered at 4000.0 angstrom with a FWHM of 40.0 angstrom in an otherwise uniform continuum.....	29
2.8	The theoretical scattered intensity spectrum by the coronal electrons for an input spectrum given by figure (2.7). The theory assumes an isothermal corona. The plots show that the smearing of the absorption line in the scattered increases with increasing temperatures.....	30



2.9	An input intensity spectrum containing two absorption lines centered at 4000.0 and 4500.0 angstroms with a FWHM of 40.0 angstrom in an otherwise uniform continuum.....	31
2.10	The theoretical scattered intensity spectrum by the coronal electrons for an input spectrum given by figure (2.9). The theory assumes an isothermal corona. The difference in the depths of the absorption lines in the scattered spectrum is due to the wavelength dependent limb-darkening coefficient.....	32
2.11	An input intensity spectrum consisting of two absorption lines centered at 4000.0 and 4500.0 angstroms while an emission line centered at 4250.0 angstrom and with a FWHM of 40.0 angstrom for the absorption and emission lines in an otherwise uniform continuum.....	33
2.12	The theoretical scattered intensity spectrum by the coronal electrons for an input spectrum given by figure (2.11). The theory assumes an isothermal corona. The difference in the depths of the absorption lines in the scattered spectrum is due to the wavelength dependent limb-darkening coefficient.....	34

2.13	This figure shows the theoretical K-coronal intensity spectra for four isothermal coronal temperatures whose electron density is given by equation (5.8). The absolute intensity of the disk center photospheric spectrum is also shown. The vertical bars at the bottom of the figure indicate the relative strengths of the three coronal lines “c”, and nine flash spectrum lines “f”. Reproduced from Cram (1976).....	37
2.14	This is a schematic drawing to illustrate the redshifting of the photospheric radiation scattered off the coronal electrons, which are radially flowing away from the sun at a uniform velocity ( $w$ ). Electron 2 is located at the closest point on the line of sight to the center of the sun. Electrons 1 and 3 are located symmetrically on either sides of electron 2.....	39
2.15	This figure shows the scale of the thermal Doppler broadening and the redshift associated with the solar wind velocity in the wavelength scale in comparison to the features of the photospheric spectrum. The scale of the redshift is shown by a red dot, which is highlighted by a circle. This comparison is made for an incident wavelength of 4000.0 angstrom on the coronal electrons, which are radially outflowing at a velocity of 300.0 km/sec in a million degree Kelvin corona.....	40
2.16	Modeled K-coronal intensity against wavelength for different isothermal coronal temperatures, for line of sight at 1.1 solar radii and a wind velocity of 400.0 km/sec.....	41

2.17	Modeled K-coronal intensity against wavelength for different isothermal coronal temperatures, for line of sight at 1.1 solar radii and a wind velocity of 800.0 km/sec.....	42
2.18	Modeled K-coronal intensity against wavelength for solar wind velocities of 0.0 km/sec to 900.0 km/sec in intervals of 100.0 km/sec, for line of sight at 1.1 solar radii and an isothermal coronal temperature of 1.0 MK.....	43
2.19	The intensity ratio at 3850.0 to 4100.0 angstroms against isothermal coronal temperatures for a range of solar wind velocities with the line of sight at 1.1 solar radii. The horizontal spread in the low end of the temperature scale is ~0.02 MK over the velocity range of 0.0 km/sec to 900.0 km/sec.....	45
2.20	The intensity ratio at 3987.0 to 4233.0 angstroms against solar wind velocities for a range of isothermal coronal temperatures with the line of sight at 1.1 solar radii. To determine the wind velocity, first the temperature has to be determined from figure (2.19). Then the K-coronal models need to be created for a range of wind velocities at this temperature and plotted in figure (2.20).....	46
3.1	Meade 12-inch, F/10.0 Schmidt-Cassegrain telescope with auto tracking capabilities.....	51
3.2	F/6.3 focal reducer reduces the focal length by a factor of 0.63. The device shown in figure (3.4) was placed at the focal plane behind the F/6.3 focal reducer.....	52

3.3	A drawing depicting the location of the fiber tips on the image plane of the telescope. The inner and outer rings are at 1.1 and 1.5 solar radii, respectively. During the eclipse the lunar shadow replaces the sun.....	53
3.4	The glass plate imbedded with twenty-one fibers. The inner and the outer circles are located at 1.1 and 1.5 solar radii, respectively, on the image plane of the sun. The fiber at the center was to record the background signal during the eclipse.....	54
3.5	This is a picture of the spectrograph. The coronal light was fed into the spectrograph by twenty-one fibers that were vertically arranged at a regular spacing. Its location in the spectrograph was at the focal point of the collimating lens.....	55
3.6	This is a picture of the inside of the spectrograph between the grating and the camera lens. Baffling were used to prevent all orders but the first order from entering into the camera lens.....	56
3.7	This is a picture of the thermoelectrically cooled CCD camera used in the experiment. The front end housed the camera lens that focused the dispersed light from the grating on to the camera.....	57
3.8	Schematic drawing on the image formation by the primary mirror of the telescope.....	59
3.9	Transmission efficiency of the fibers used in MACS and marked as UV/VIS. The region of wavelength interest in MACS was from 3500.0 –4500.0 angstroms.....	62

3.10	Schematic diagram depicting the light ray path at the focal plane of the telescope into a fiber optic cable.....	<b>63</b>
3.11	Reflection properties for the anti UV-reflective coating on the collimating and the camera lenses used in the spectrograph.....	<b>66</b>
3.12	Transmission properties at normal incidence for the anti UV-reflection coating on the transmission grating. Here the back surface reflection is not considered. The substrate material is fused silica. The black squares pertain to the grating used in MACS.....	<b>67</b>
3.13	Quantum efficiency (QE) curve for the back thinned SITE 512.0×512.0, 24.0mm square chip used in MACS. This chip also featured a full well depth in excess of 300,000.0 electrons, a dynamic range of ~ 90.0 dB and a readout time of ~ 5.0 seconds with an ISA card.....	<b>68</b>
3.14	Schematic diagrams of the optical components that make up MACS and the parameters that determine the spatial and the spectral resolutions.....	<b>69</b>
3.15	Schematic diagram showing the projected width and height of a single fiber on the camera plane.....	<b>71</b>
3.16	Schematic diagram of the dispersing element showing the angular and the linear dispersions.....	<b>72</b>
3.17	Schematic layout of the slit spectrometer. In this diagram collimated light is incident on the grating.....	<b>73</b>
3.18	Schematic diagrams showing the diffraction limited spectral resolution and the resolving power.....	<b>76</b>

4.1	A photograph of the August 1999 eclipse from the Black Sea area. The photograph also reveals a detached prominence eruption above the southwest limb.....	89
4.2	A map showing the path of the eclipse over Turkey. Courtesy: NASA Reference Publication 1398.....	89
4.3	A picture showing the layout of MACS and the telescope. The telescope is on a polar mount and MACS is laid out on the metal box.....	90
4.4	The spectra from twenty-one fibers exposed to the sky while four other fibers exposed to the mercury calibration lamp in Elazig, Turkey.....	91
4.5	The coronal spectra recorded by MACS for the exposure times 4.0, 8.0 and 83.0 seconds, respectively. Each vertical line corresponds to a spectrum from a single fiber. It is also clear that five of the fibers show emission lines...	93
4.6	This picture shows the envisaged location of the twenty-one fibers in the focal plane during the eclipse. The inner and the outer rings correspond to 1.1 and 1.5 solar radii, respectively. The picture is not the actual eclipse on 11 August 1999. The fiber in the center was expected to record the background signal.....	94
4.7	The spectrum recorded by the fiber #19 in the 4.0 seconds exposure. The emission lines and their corresponding wavelengths and pixel positions are identified.....	97
4.8	The regression fit between the emission line peaks and the peak positions of the fiber #19 in the 4.0 seconds exposure. The table incorporated shows the wavelength scale between any two-emission lines.....	98

4.9	The spectrum recorded by the fiber #20 in the 4.0 seconds exposure. This too matches with all the emission lines recorded by the fiber #19 as shown in figure (4.7).....	<b>99</b>
4.10	The spectrum recorded by the fiber #22 in the 4.0 seconds exposure. The emission lines and their corresponding wavelengths and pixel positions are identified.....	<b>101</b>
4.11	The regression fit between the emission line peaks and the peak positions of the fiber #19 in the 4.0 seconds exposure. The table incorporated shows the wavelength scale between any two-emission lines.....	<b>102</b>
4.12	This is a comparison between solar image by SOHO in 304.0 angstrom at 11:14 UT and an eclipse photograph taken from the Black Sea at ~ 11:16UT. The orientation was made by matching the prominence eruption ~ 68 <sup>0</sup> southwest in the SOHO image. The orientation of the polar axis of the sun with respect to the polar axis of the earth was obtained from the p-angle data given in, ‘The Astronomical Almanac 1999’ for 11 August 1999.....	<b>104</b>
4.13	Images of the sun taken by the LASCO instrument on SOHO on the 11 August 1999. The numbers denote the time in UT. C2 and C3 are coronal images of the sun from 2.0 – 6.0 solar radii and 3.7 – 32.0 solar radii, respectively, using an externally occulted disk.....	<b>105</b>
4.14	Images of the sun taken by the EIT instrument on SOHO on the 11 August 1999. The numbers denote the time in UT.....	<b>106</b>

4.15	Images of the sun taken by the radiograph in Nancy, France and the x-ray telescope on Yohkoh on the 11 August 1999.....	<b>107</b>
4.16	Plots of the sky spectrum recorded by fiber #06 in Elazig, Turkey before and after correcting for Rayleigh scattering. The plots have been normalized at 3968.5 Angstrom.....	<b>109</b>
4.17	Plots of the extraterrestrial photospheric intensity spectrum and the terrestrial photospheric intensity spectrum recorded by fiber #06. The extraterrestrial photospheric spectrum is a smoothed version of the extraterrestrial photospheric spectrum shown in figure (2.1).....	<b>110</b>
4.18	Plots of the smoothed extraterrestrial photospheric intensity spectrum and the terrestrial photospheric intensity spectrum recorded by fiber #06.....	<b>111</b>
4.19	Plots of the smoothed extraterrestrial photospheric intensity spectrum, terrestrial photospheric intensity spectrum recorded by fiber #06 and the ratio between these two against wavelength.....	<b>112</b>
4.20	Polynomial fit made to the ratio between the extraterrestrial photospheric spectrum and the terrestrial photospheric intensity spectrum. The numbers on the plot are the coefficients of the polynomial fit.....	<b>113</b>
4.21	Application of the polynomial fit shown in figure (4.20) to the terrestrial photospheric intensity spectrum to obtain the extraterrestrial photospheric intensity. Also plotted for comparison purpose is the smoothed extraterrestrial photospheric intensity spectrum as shown in figure (4.18).....	<b>114</b>



4.22	These plots show the coronal spectra recorded by the twenty-one fibers located at various latitudes and heights on the corona as depicted in figure (4.12). Fiber #23 was centered on the moon. The above spectra were recorded in the 18.0 seconds exposure. The x-coordinate is in pixel units.....	<b>117</b>
4.23	The coronal spectrum recorded by fiber #06.....	<b>119</b>
4.24	The terrestrial K-coronal spectrum reduced from the coronal spectrum recorded by fiber #06.....	<b>120</b>
4.25	This plot shows the extraterrestrial K-coronal spectrum derived for fiber #06. The wind and the temperature sensitive intensity ratios are 1.245 and 1.488, respectively.....	<b>121</b>
4.26	The temperature sensitive plot. This assigns a thermal electron temperature of ~1.73 MK for fiber #06.....	<b>122</b>
4.27	The wind sensitive plot. This assigns a solar wind velocity of ~467.0 km/sec for fiber #06.....	<b>122</b>
4.28	The temperature sensitive plot. This assigns a thermal electron temperature of ~1.29 MK for fiber #04.....	<b>123</b>
4.29	The wind sensitive plot. This assigns a solar wind velocity of ~300.0 km/sec for fiber #04.....	<b>123</b>
4.30	This plot shows the extraterrestrial K-coronal spectrum for fiber #10. The wind and the temperature sensitive intensity ratios are 1.248 and 1.524, respectively.....	<b>124</b>

4.31	The temperature sensitive plot. This assigns a thermal electron temperature of ~1.34 MK for fiber #10.....	<b>125</b>
4.32	The wind sensitive plot. This assigns a solar wind velocity of ~571.0 km/sec for fiber #10.....	<b>125</b>
4.33	This plot shows the terrestrial coronal spectrum recorded by fiber #14. The continuum is a measure of the terrestrial F+K corona. The E-corona is removed by making Gaussian fits of the form given in equation (4.1) to the individual emission lines and fitting the background given by equation (4.2) to the continuum.....	<b>126</b>
4.34	This plot shows the extraterrestrial K-coronal spectrum for fiber #14. This is following the elimination of the E-corona from figure (4.33).....	<b>127</b>
4.35	The temperature sensitive plot. This assigns a thermal electron temperature of ~0.73 MK for fiber #14.....	<b>128</b>
4.36	The wind sensitive plot. This assigns a solar wind velocity of ~819.0 km/sec for fiber #14.....	<b>128</b>
4.37	Plot showing the variation in the temperature-sensitive intensity ratio, from the theoretical models without streamers, for a streamer of geometry described in Appendix-C and density enhanced by a factor of 50.0 together with various streamer inclinations in front and behind the solar limb.....	<b>129</b>

4.38	The thermal electron temperature and the solar wind velocity determined for solar coronal locations observed by fibers #04, 06, 08, 10, 12, 14 & 22 that are located at 1.1 solar radii and fiber #15 & 17 located at 1.5 solar radii. These values are based on the theoretical models. The temperature and the wind velocity are measured in MK and km/sec, respectively. However the wind measurements seem too far high. In this regard it is acknowledged that the experiment was not successful in measuring the wind velocities and the absolute values should be disregarded.....	<b>131</b>
4.39	The spectrum recorded by fiber #23, which was centered on the lunar shadow during the eclipse. Its purpose was to measure the background counts.....	<b>132</b>
5.1	This is a schematic diagram showing the mathematical description of the scattering phenomenon where the photospheric radiation from the sun is scattered by the free electrons lying along the line of sight of an observer. The line of sight is at a distance ( $r$ ) from the center of the sun.....	<b>137</b>
5.2	A plot showing the solar radial log-intensity variation as a function of solar radii ( $r$ ) from the center of the sun. The solid curve represents the measurements by November and Koutchmy (1996) while the dashed curve represents the measurements by Baumbach (1937) based on several eclipses observations.....	<b>142</b>

5.3	A plot showing the log of the electron density variation as a function of the solar radii ( $r$ ) from the center of the sun. The solid curve represents the calculations by November and Koutchmy (1996) while the dashed curve represents the calculations by Baumbach (1937) based on several eclipses observations.....	<b>143</b>
5.4	A photograph of the solar corona during the total solar eclipse of 11 August 1999 where the sun was approaching the maximum phase. Here the corona is uniformly bright and circular in shape.....	<b>144</b>
5.5	A photograph of the solar corona during the total solar eclipse of 4 November 1994 where the sun was approaching the minimum phase. Here the corona is elongated in the equatorial regions and brighter than the polar regions.....	<b>144</b>
5.6	A series of plots showing the radial dependence of the mean electron density in coronal holes computed from various sets of polarization brightness data. This plot was obtained from Cranmer et al. (1999).....	<b>148</b>
5.7	A plot showing the electron densities for the north (solid line) and south polar coronal holes (dashed line) and the north (dotted line) and south (dot-dashed line) polar coronal rays as a function of height. Reproduced from Fisher and Guhathakurta (1995).....	<b>151</b>

5.8	A comparison of the electron number density functions based on the models by Baumbach (1937, equation (5.7)), Ichimoto et al. (1996, equation (5.8)), Newkirk (1961, equation (5.9)), Cranmer et al. (1999, equation (5.10)) and Guhathakurta and Holzer (1994, equation (5.12)).....	<b>152</b>
5.9	Plots of the theoretical K-coronal intensity spectra based on the electron number density functions given by Baumbach (1937, equation (5.7)), Ichimoto et al. (1996, equation (5.8)), Newkirk (1961, equation (5.9)), Cranmer et al. (1999, equation (5.10)) and Guhathakurta and Holzer (1994, equation (5.12)) and the line of sight at 2.0 solar radii from the center of the sun. The curves have been normalized at 4000.0 angstrom.....	<b>153</b>
5.10	Plots of the theoretical K-coronal intensity spectra based on the electron number density functions given by Baumbach (1937, equation (5.7)), Ichimoto et al. (1996, equation (5.8)), Newkirk (1961, equation (5.9)), Cranmer et al. (1999, equation (5.10)) and Guhathakurta and Holzer (1994, equation (5.12)) and the line of sight at 1.1 solar radii from the center of the sun. The curves have been normalized at 4000.0 angstrom....	<b>154</b>
5.11	This is a plot of the temperature profile along the line of sight at 1.3 solar radii based on the assumption of a conductive corona Chapman (1957). The temperature at the point of intersection of the line of sight and the plane of the solar limb is 1.0 MK.....	<b>156</b>

5.12	This is a plot of the modeled K-coronal intensity spectra for an isothermal corona of 1.0 MK and a model with the temperature profiles given by $T(r) = 1.0 \cdot (1.3/r)^{2/7}$ and $T(r) = 1.0 + (1.0 + 9.0 \cdot (r - 1.75)^2)^{-1}$ . Here (r) is the distance between the center and points along the line of sight 1.3 solar radii. The temperature at the point of intersection of the line of sight and the plane of the solar limb is 1.0 MK.....	<b>157</b>
5.13	Coronal wind profile based on the Parker model for an isothermal corona. In the ideal solution the velocity is equal to the isothermal sound speed at the critical radius and starts with subsonic velocities at the lower boundary and reaches supersonic velocities at large distances.....	<b>159</b>
5.14	Comparison of the theoretical K-coronal intensity spectrum for an isothermal corona at 1.0 MK, zero wind velocity and line of sight at 1.5 solar radii with the intensity spectrum due to the bulk flow velocity that naturally arises with the Parker wind model for an isothermal corona as given in equation (5.14).....	<b>160</b>
5.15	Comparison between two theoretical K-coronal intensity spectra due to isothermal coronal temperatures of 1.0 and 1.5 MK and with the inclusion of the Parker wind model for an isothermal corona.....	<b>161</b>

5.16	Plot of the polarization from theoretical modeling for the formation of the K-corona, at a given isothermal coronal temperature of 1.0 MK, for lines of sight at 1.1, 1.3 and 1.5 solar radii. The behavior of the polarization conforms to the observations. That is, the polarization is almost wavelength independent and increases with coronal heights.....	<b>163</b>
6.1	The spectrum recorded by the fiber located in the center of the lunar shadow during the eclipse. The x-coordinate corresponds to wavelength scale. The two prominent peaks are associated with the Calcium K & H lines corresponding to 3933.7 and 3968.5 angstroms, respectively.....	<b>168</b>
6.2	Theoretical isothermal K-coronal models fitted to the observed K-coronal intensity spectrum to determine the temperature by Ichimoto et al. (1996). The lower curves show the differences between the observational spectrum and the theoretical models. The model that showed the least difference determined the temperature.....	<b>169</b>

6.3	This plot shows the comparison between experimentally obtained K-coronal spectrum for fiber # 04 with theoretical models for various isothermal temperatures. From the intensity ratio method the wind velocity and the temperature deduced for fiber # 04 are, 300.0 km/sec and 1.29 MK, respectively. The theoretical K-coronal models plotted in figure (6.3) correspond to a wind velocity of 300.0 km/sec and isothermal coronal temperatures of 0.5MK, 1.0 MK, 1.5 MK and 2.0 MK. In such a scenario the experimentally obtained K-coronal spectrum may be expected to take a position between the theoretical models for 1.0 MK and 1.5 MK. (Expt: = Experimental, Theo: Theoretical).....	<b>172</b>
6.4	A plot of the superposition of figure (6.1) and figure (6.3). The shape of the spectrum recorded by the fiber located in the center of the lunar shadow corresponds with the shape of the observed K-coronal spectrum by fiber #04. The expected location of the observed spectrum is between the theoretical isothermal K-coronal spectra for 1.0 MK and 1.5 MK.....	<b>174</b>
6.5	A plot showing the observed K-coronal spectrum for fiber #04 along with the theoretical K-coronal spectrum for the wind velocity and temperature derived from fiber #04. The plot also includes the difference between the observational and the theoretical plots along with the scattered light spectrum observed by the fiber in the center of the lunar shadow.....	<b>175</b>



6.6	Plots showing the effect on the shape of the observed K-coronal spectrum of fiber # 04, as shown in figure (6.5), in comparison with the shape of the theoretical K-coronal spectrum by subtracting various fractions of the scattered spectrum from the observed K-coronal spectrum. A, B, C, D, E and F correspond to a subtraction of 0.0%, 15.0%, 10.0%, 8.0 %, 5.0% and 3.0%, respectively, of the scattered light spectrum recorded by the fiber that was located in the center of the lunar shadow from the spectrum recorded by fiber #04. These plots show that the observed spectrum closely follows the shape of the theoretical spectrum with various fractional subtraction of the scattered spectrum.....	<b>178</b>
6.7	The extra fibers placed in the shadow of the moon and outside the field of view in order to record the instrumental stray light distribution.....	<b>181</b>
6.8	A schematic diagram showing the introduction of a very thin high transmission glass surface (AB) inclined at $45^0$ to the optical axis with a semi-reflecting coating on the side facing the fiber optic plate along with the fibers embedded on an optical flat. This alteration will enable the simultaneous imaging of the image formed on the fiber optic plate.....	<b>184</b>

7.1	The path envisaged for the unmanned Solar Probe Spacecraft. At the perihelion (C) and the poles the spacecraft will be four and eight solar radii, respectively, from the center of the sun. The position of the spacecraft (P) is given by $(r, \mathbf{Q})$ with respect to the center of the sun. In this picture the parabolic path, the detector plane and the center of the sun are in the same plane.....	188
7.2	The theoretical K-coronal intensity variation for various detector elevations for 0.0 km/sec wind velocity and the spacecraft positioned at the pole (P).....	192
7.3	The theoretical K-coronal intensity variation for various detector elevations for 400.0 km/sec wind velocity and the spacecraft positioned at the pole (P)...	192
7.4	The variation of the wind-sensitive intensity ratio against $g$ for various wind velocities at $T=1.0$ MK and the spacecraft positioned at the pole.....	193
7.5	The variation of the temperature-sensitive intensity ratio against $g$ for various temperatures at $W=400.0$ km/sec and the spacecraft positioned at the pole.....	193
7.6	Temperature-sensitive intensity ratioVS Temperature for various wind velocities at $g = 0.0$ degrees and the spacecraft positioned at the pole.....	194
7.7	Wind-sensitive intensity ratioVS Wind velocity for various temperatures at $g = 0.0$ degrees and the spacecraft positioned at the pole.....	194
7.8	Temperature-sensitive intensity ratioVS Temperature for various wind velocities with intensities measured through filters of fifty angstrom bandpass centered at those wavelengths for line of sight at 1.1 solar radii.....	195

7.9	Wind-sensitive intensity ratioVS Wind velocities for various temperatures with intensities measured through filters of fifty angstrom bandpass centered at those wavelengths for line of sight at 1.1 solar radii.....	196
A.1	The general coordinates where $\mathbf{r}$ is a field point and $\mathbf{r}'$ is a source point.....	197
A.2	The general coordinates of the incident and scattered radiation and the orientations of the parallel and the perpendicular components of the electric vectors with respect to the scattering plane.....	206
A.3	Propagation of a monochromatic plane EM waves.....	210
A.4	Coordinates for the rotational transformation of the scattering plane through an angle $\alpha$ about the line of sight.....	212
A.5	Geometrical configuration for the scattering of photospheric radiation by coronal electrons.....	214
A.6	Geometrical configuration for the formation of the K- Corona. Photospheric radiation emitted from a point S on the Sun is scattered from an electron E towards an observer O. The solar wind on the electron is radial and blows in the direction CE.....	215
A.7	Scattering of radiation off an electron also known as Compton scattering.....	216
A.8	Construction to obtain an expression for the scattered intensity in the rest frame of the observer. Consider a coronal electron with velocity $\mathbf{u}$ subjected to radial solar wind velocity $\mathbf{w}$ in a coordinate system where the x-axis bisects the supplement of the scattering angle.....	219
A.9	Highlighted map of the radial and the scattering planes of figure (A.6).....	226

A.10	Highlight of the spherical triangle formed by EDJI in figure (A.6).....	228
A.11	Highlight of the triangle ESC of figure (A.6).....	229
B.1	The plot of extraterrestrial solar irradiance VS wavelength obtained with a Fourier Transform Spectrometer at the McMath/Pierce Solar Telescope on Kitt Peak, Arizona.....	247
B.2	The plot of limb-darkening coefficient versus wavelength with linear approximation super imposed.....	248
B.3	The plot of electron number density versus the radial distance from the solar surface for the two models given by equation (B.31) and equation (B.32).....	251
B.4	Illustrating the integration procedure of the first integral in equation (B.44)...	261
B.5	Plot of the cumulative y-axis values of figure (B.4) against the wavelength $h\nu$ .....	262
C.1	Model streamer of thickness $d$ in front of the solar limb with an electron density enhancement by a factor $f_s$ and thermal electron temperature $T_s$ .....	277
C.2	Plot to show the effect of streamers on the K-coronal spectrum with $d=0.5$ SR, $f_s=4.0$ , $T_s=T=1.0$ MK and at angles $\theta = -45.0$ and $+45.0$ degrees.....	280
C.3	Model streamers of similar dimensions at $-45.0$ and $+45.0$ degrees above and below the plane of the solar limb, respectively.....	281
C.4	Plot to show the effect of streamers on the K-coronal spectrum with $d=0.5$ SR, $f_s=4.0$ , $T_s=T=1.0$ MK and spread over various angles $\theta$ .....	282

C.5	Effects by streamers on the ratio $I(4233)/I(3987)$ for $W=400$ km/sec and $\rho=1.1$ SR. The horizontal lines show the intensity ratio for a given solar wind velocity of 400.0 km/sec and line of sight at 1.1 solar radii, and for different isothermal coronal temperature in the absence of streamers.....	<b>283</b>
C.6	Effects by streamers on the ratio $I(4100)/I(3850)$ for $W=400$ km/sec and $\rho=1.1$ SR. The horizontal lines show the intensity ratio for a given solar wind velocity of 400.0 km/sec and line of sight at 1.1 solar radii, and for different isothermal coronal temperature in the absence of streamers.....	<b>284</b>

## **Abstract**

The determination of the radial and latitudinal temperature and wind profiles of the solar corona is of great importance in understanding the coronal heating mechanism and the dynamics of coronal expansion. Cram (1976) presented the theory for the formation of the K-coronal spectrum and identified two important observations. He observed the existence of temperature sensitive anti-nodes at certain wavelengths in the theoretical K-coronal spectra. The anti-nodes are separated by temperature-insensitive nodes. Remarkably, Cram showed that the wavelengths of the nodes and anti-nodes are almost independent of altitude above the solar limb. Because of these features, Cram suggested that the intensity ratios at two anti-nodes could be used as a diagnostic of the electron temperature in the K-corona. Based on this temperature diagnostic technique prescribed by Cram a slit-based spectroscopic study was performed by Ichimoto et.al (1996) on the solar corona in conjunction with the total solar eclipse of 3 November 1994 in Putre, Chile to determine the temperature profile of the solar corona. In this thesis Cram's theory has been extended to incorporate the role of the solar wind in the formation of the K-corona, and we have identified both temperature and wind sensitive intensity ratios. The instrument, MACS, for Multi Aperture Coronal Spectrometer, a fiber optic based spectrograph, was designed for global and simultaneous measurement of the

thermal electron temperature and the solar wind velocity in the solar corona. The first ever experiment of this nature was conducted in conjunction with the total solar eclipse of 11 August 1999 in Elazig, Turkey. In this instrument one end of each of twenty fiber optic tips were positioned in the focal plane of the telescope in such a way that we could observe conditions simultaneously at many different latitudes and two different radial distances in the solar corona. The other ends of the fibers were vertically aligned and placed at the primary focus of the collimating lens of the spectrograph to obtain simultaneous and global spectra on the solar corona. By isolating the K-coronal spectrum from the spectrum recorded by each fiber the temperature and the wind sensitive intensity ratios were calculated to obtain simultaneous and global measurements of the thermal electron temperature and the solar wind velocity. We were successful in obtaining reliable estimates of the coronal temperature at many positions in the corona. This is the first time that simultaneous measurements of coronal temperatures have been obtained at so many points. However due to instrumental scattering encountered during observations, reliable estimates of the wind velocity turned out to be impossible to obtain. Although remedial measures were taken prior to observation, this task proved to be difficult owing to the inability to replicate the conditions expected during an eclipse in the laboratory. The full extent of the instrumental scattering was apparent only when we analyzed the observational sequence. Nevertheless the experience obtained from this very first attempt to simultaneously and globally measure both the wind velocity and the temperature on the solar corona have provided valuable information to conduct any future observations successfully.